Single-molecule spectroscopy of protein folding in a chaperonin cage

Hagen Hofmann[a], Frank Hillger[a], Shawn H. Pfeil[b], Armin Hoffmann[a], Daniel Streich[a], Dominik Haenni[a], Daniel Nettels[a], Everett A. Lipman[b], and Benjamin Schuler[a,1]

[a]Biochemisches Institut, Universität Zürich, Winterthurerstrasse 190, 8057 Zürich, Switzerland; and [b]Department of Physics, University of California, Santa Barbara, CA 93106

Molecular chaperones are known to be essential for avoiding protein aggregation in vivo, but it is still unclear how they affect protein folding mechanisms. We use single-molecule Förster resonance energy transfer to follow the folding of a protein inside the GroEL/GroES chaperonin cavity over a time range from milliseconds to hours. Our results show that confinement in the chaperonin decelerates the folding of the C-terminal domain in the substrate protein rhodanese, but leaves the folding rate of the N-terminal domain unaffected. Microfluidic mixing experiments indicate that strong interactions of the substrate with the cavity walls impede the folding process, but the folding hierarchy is preserved. Our results imply that no universal chaperonin mechanism exists. Rather, a competition between intra- and intermolecular interactions determines the folding rates and mechanisms of a substrate inside the GroEL/GroES cage.

chaperone | confinement | microfluidic mixing | FRET | fluorescence

In the recent past, a large number of components have been identified that control and modulate protein folding in vivo. This machinery includes molecular chaperones (1–3), sophisticated quality control systems, and complex mechanisms for protein translocation and degradation (3, 4), reflecting the importance of regulating the delicate balance of protein folding, misfolding, and aggregation in the cell. Such cellular factors exert conformational constraints on protein molecules that are expected to have a strong effect on the corresponding free-energy surfaces for folding (5). However, while the combination of cellular, biochemical, and structural data has led to some plausible qualitative models for the processes involved, mechanistic investigations comparable to those of autonomous protein folding in vitro (5–8) have been complicated by the complexity of the systems and the conformational heterogeneity involved (9). Even the autonomous folding of chaperone substrate proteins has been difficult to investigate because of their strong aggregation tendency (10). Contributions from confinement and crowding have been addressed in numerous studies using molecular simulations and theory (11–20), but many of these concepts have eluded experimental examination.

Here, we take a step towards closing this gap by investigating the GroEL/GroES chaperonin (1–3, 9) with single-molecule fluorescence spectroscopy (21–24), a method that is starting to provide previously inaccessible information on chaperone-mediated protein folding (25–30). GroEL/GroES is a remarkable molecular machine that binds nonnative proteins and allows them to fold within a cavity formed by the heptameric rings of GroEL and GroES. However, the cavity is only slightly larger than the folded structure of typical proteins known to interact with the chaperonin. The large volume of unconfined unfolded protein chains compared to the size of the cavity raises the question of whether and how such strong confinement affects the folding reaction (12–16, 18, 31, 32). By labeling the classic substrate protein rhodanese (33) with donor and acceptor fluorophores, we can follow the folding reaction with multiparameter single-molecule Förster resonance energy transfer (FRET) (34) and probe the folding pathway of rhodanese inside and outside the chaperonin cavity in much greater detail than previously possible.

Results and Discussion

Chaperone-Mediated Protein Folding Observed with Single-Molecule FRET. To achieve an optimal discrimination of native and nonnative conformations, three variants of the two-domain protein rhodanese were investigated. Two fluorophores (Alexa Fluor 488 and Alexa Fluor 594) were attached to each variant to map the folding of the N-terminal domain (N variant), the structure formation of the linker separating both domains (L variant), and the folding of the C-terminal domain (C variant) (Fig. 1A). Fig. 1B shows histograms of the transfer efficiency E for all three rhodanese variants, determined from photon bursts of individual rhodanese molecules freely diffusing through the observation volume of the confocal instrument. Under native conditions (Fig. 1B), two peaks are observed for each variant: the peaks at $E = 0.67$ for the N variant, $E = 0.69$ for the L variant (27), and $E = 0.98$ for the C variant result from native rhodanese molecules; the peaks near $E = 0$ result from molecules lacking an active acceptor dye and can be eliminated by dual color excitation of donor and acceptor (35, 36) (Fig. 1B, see *SI Appendix* for details). When the refolding of rhodanese is initiated in the presence of GroEL, rhodanese binds to the chaperonin ring, resulting in characteristic broad transfer efficiency distributions for all three variants with maxima at $E > 0.8$ (Fig. 1B), whose width originates predominantly from static orientational heterogeneity of the fluorophores (27). To investigate refolding inside the chaperonin cavity, we use the single ring variant of GroEL (SR1), which resembles the folding active state of GroEL, but does not release the substrate protein (37, 38). Upon incubation of the SR1-rhodanese complex with ATP and the cochaperone GroES, stable complexes assemble (*SI Appendix: Fig. S1*), and rhodanese is displaced into the cavity formed by SR1 and GroES within a few seconds (31, 37). During the folding of rhodanese inside the chaperonin cage, we observe that the transfer efficiency histograms of all variants approach the histograms of the free native state (Fig. 1B). The concurrent decrease in the donor and acceptor fluorescence anisotropies (*SI Appendix: Fig. S2*) indicates an increase in rotational freedom of the fluorophores during folding, a behavior observed previously during release of substrate proteins into the cavity (31, 37). Even though some residual broadening from static orientational heterogeneity of the fluorophores remains in the encapsulated folded state, the characteristic changes in the transfer efficiency histograms allow us to follow the folding of rhodanese inside the
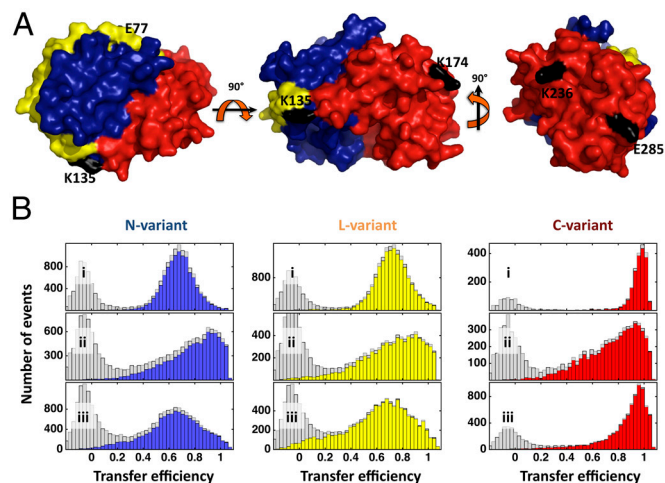
Fig. 1. Native structure and transfer efficiency histograms of the rhodanese variants. (*A*) Surface representation of rhodanese showing the N-terminal domain (*blue*), the interdomain linker (*yellow*), and the C-terminal domain (*red*) (protein data bank entry 1rhs). The rhodanese variants E77C/K135C (*N variant*), K135C/K174C (*L variant*), and K236C/E285C (*C variant*) were labeled with Alexa Fluor 488 as a donor and Alexa Fluor 594 as an acceptor. Label attachment sites are indicated in *black*. (*B*) Transfer efficiency histograms of native rhodanese (*i*), the SR1-rhodanese complex (*ii*), and the SR1-rhodanese complex 1.5 h after addition of GroES and ATP (*iii*). The gray histograms were recorded with donor excitation only; the colored histograms were recorded using dual color excitation of donor and acceptor (35, 73) to eliminate the contribution close to $E = 0$ from molecules lacking an active acceptor dye.

GroEL cage and compare the kinetics with those of its autonomous refolding in solution.

Folding Kinetics Outside and Inside the Cage. Autonomous refolding of rhodanese was initiated by manually diluting unfolded rhodanese (4 M guanidinium chloride) into native conditions. Chaperone-mediated refolding was triggered by mixing the binary rhodanese-SR1 complex with GroES (1 μM) and ATP (2 mM). The single-molecule fluorescence signal was recorded until the refolding reaction was complete, typically for 2 h. To obtain time-resolved FRET efficiency histograms, we performed a moving window analysis by splitting the single-molecule recordings into short intervals of equal duration (50 s for the autonomous folding of the C variant and 300 s for all other variants) (Fig. 2*A*, see *SI Appendix* for details). For both the autonomous and the SR1-mediated folding reactions of all variants, transfer efficiency histograms characteristic of native molecules developed during the measurements (Fig. 2*A*).

For the autonomous folding of rhodanese, it might appear feasible to analyze the kinetics of the histograms in terms of two well-defined states, but the broad histograms of the chaperone-mediated reaction obviously require a less model-dependent analysis. We thus employed singular value decomposition (SVD), which can be used to factorize a matrix representation of the experimental data into a minimal set of basis vectors and amplitude vectors, whose linear combination, weighted by the corresponding singular values, can be used to represent the data (39). In our case, we can analyze the change of the two-dimensional histograms with time to determine the kinetics and the minimum number of distinguishable molecular species required for describing the folding process without loss of information (see *SI Appendix* for details). All nine experimentally accessible observables, represented in two-dimensional histograms (*SI Appendix: Fig. S3–5*), were combined in one global SVD analysis (Fig. 3*C*, *D* and *SI Appendix: Fig. S6–8*). While parameters such as transfer efficiency and burst duration are more sensitive to global changes in the dimension of the protein, fluorescence lifetime and fluorescence anisotropy report on changes in the local environment and
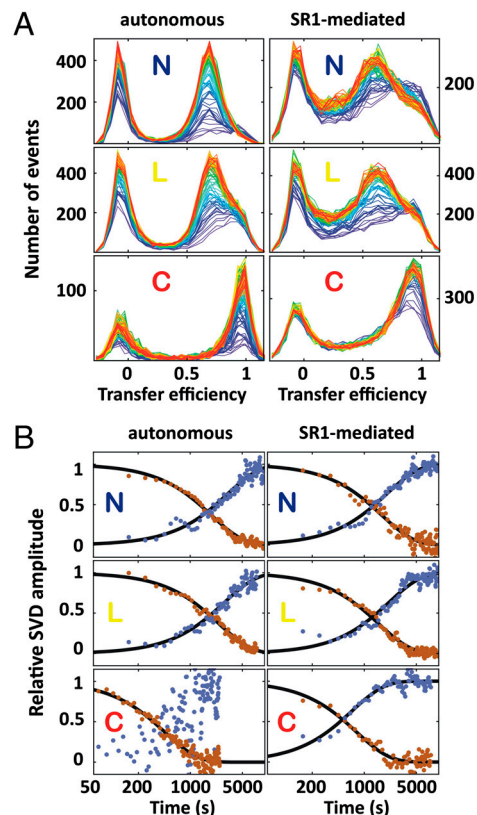

Fig. 2. Kinetic analysis of the autonomous and chaperone-mediated rhodanese refolding reactions using SVD. (*A*) Transfer efficiency histograms as a function of time (*progressing from blue to red*) of the autonomous (*Left*) and SR1-mediated (*Right*) folding reaction for N variant, L variant, and C variant (from *Top* to *Bottom*) at 24 °C. (*B*) Kinetics from the first (*red*) and second (*blue*) amplitude vectors of the SVD for the autonomous (*Left*) and SR1-mediated (*Right*) folding reaction of the N variant, L variant, and C variant.

the rotational freedom of the fluorophores, respectively. The basis vectors contain information about the parts of the histograms that change over time, and the amplitude vectors report on the corresponding kinetics. Fig. 3 *C* and *D* show examples of the multidimensional SVD for the autonomous and chaperone-mediated folding reaction of the L variant at 24 °C. Interestingly, for all observables, the signal change is dominated by the first two SVD components (Fig. 3 *C* and *D* and *SI Appendix: Fig. S6–9*). The first component captures mainly an increase in the molecular brightness over time (Fig. 3 *A*, *B*, S6–8), which is probably caused by the burial of tryptophan residues in the native structure that quench donor and acceptor in the denatured state (40). The second component corresponds to the changes in all other spectroscopic parameters, e.g., the transfer efficiency (Fig. 3 and *SI Appendix: Fig. S6–8*). The two SVD components yielded very similar rate constants for each of the individual folding reactions (Fig. 2*B*), indicating the dominance of two distinguishable molecular species*. In all cases, the SVD amplitude vectors were well described by single exponential relaxations.

A comparison of the resulting rate constants for the autonomous folding of the rhodanese variants (Fig. 2*B*) suggests a simple folding mechanism. The folding rate constant of the N-terminal domain $(4.2 \pm 1.4)10^{-4}$ s^{-1} coincides with the formation of the native linker structure $(3.9 \pm 1.2)10^{-4}$ s^{-1}, but the C-terminal domain folds almost six times faster $(2.3 \pm 0.6)10^{-3}$ s^{-1} at 24 °C, indicating that the C-terminal domain folds prior to the N-terminal

---

*For the autonomous folding of the C variant, only the first component contains kinetic information because of the overlap of native and nonnative populations in the histograms.
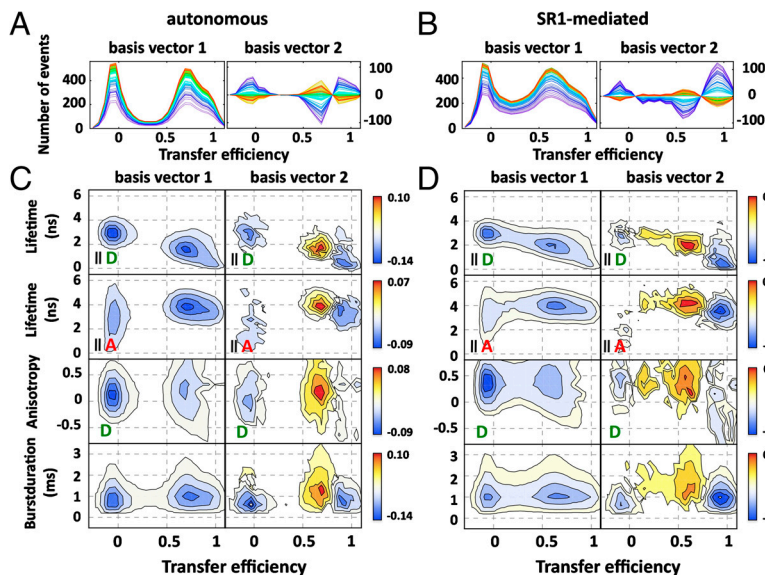
Fig. 3. Examples of basis vectors from multidimensional SVD for the autonomous and SR1-mediated folding reactions of the L variant. (*A, B*) Time evolution (*progressing from blue to red*) of the first (*Left*) and second (*Right*) one-dimensional-basis vectors for the autonomous (*A*) and SR1-mediated folding (*B*) of the L variant. Note that the one-dimensional-basis vectors shown here are just one possible projection of the multidimensional basis vectors on the transfer efficiency dimension to illustrate the kinetics. (*C, D*) Examples of two-dimensional-basis vectors from multidimensional SVD for the autonomous (*C*) and SR1-mediated (*D*) folding reactions of the L variant (*from Top to Bottom*: donor and acceptor fluorescence lifetime, donor fluorescence anisotropy, duration of bursts). The color code indicates the absolute SVD amplitude (*see color scale*). The basis vectors indicate the positions of changes of the corresponding observables in the histograms and are ordered according to their singular values.

domain. This interpretation is further corroborated by limited proteolysis experiments (*SI Appendix: Fig. S10*), excluding a dominant effect of the fluorophores on the folding mechanism[†]. Interestingly, the folding hierarchy of the domains is preserved in the highly confined space of the GroEL/GroES complex. Correspondingly, the basis vectors for autonomous and chaperone-mediated folding are similar (Fig. 3 and *SI Appendix: Fig. S6–8*). However, the folding rates of the domains are affected differently by the chaperonin cavity: the folding rate constant of the N-terminal domain $(4.5 \pm 1.2)10^{-4}$ s^{-1} and the rate constant for formation of the native linker $(5.5 \pm 1.1)10^{-4}$ s^{-1} are not changed by the chaperonin environment (Fig. 2*B*, 4*A*). In contrast, folding of the C-terminal domain is decelerated by a factor of two inside the chaperonin cavity at 24 °C $(1.0 \pm 0.4)10^{-3}$ s^{-1} (Fig. 2*B*, 4*A*); this effect increases to an eightfold deceleration when extrapolated to 37 °C (Fig. 4*A*). Even though our values for the rate constants (*SI Appendix: Fig. S11*) lie within the range of previous results obtained by enzymatic assays, a rigorous comparison to published results is complicated by the considerable spread of the rate constants reported (10, 32, 37, 41, 42). Possible reasons for this variability are the pronounced sensitivity of the system to solution conditions (10, 37), temperature (Fig. 4*A*), and difficulties in completely eliminating aggregation at the protein concentrations required in ensemble experiments (10). Importantly, aggregation in single-molecule experiments is not only improbable because of the low protein concentrations used, but it can also be monitored stringently in situ (43) and can thus be excluded for all measurements (*SI Appendix: Fig. S12*).

Rapid Kinetics from Microfluidic Mixing. A complete picture of the conformational dynamics of rhodanese during refolding requires an investigation on all biologically relevant time scales from milliseconds to hours. While the time range of minutes to hours is accessible with the above-described manual mixing experiments, recent advances in the development of continuous-flow microfluidic mixing devices (44–47) allow us to study folding reactions on the single-molecule level from milliseconds to seconds. Here, we use a microfluidic mixer designed specifically for single-molecule measurements of fast protein folding kinetics (46). A sample solution in the inlet channel containing SR1-bound rhodanese (Ch2, Fig. 5*A*) was mixed with buffer containing ATP and GroES that entered from the two side channels (Ch1 and Ch3, Fig. 5*A*). By placing the confocal volume at different positions

along the observation channel (Ch4), we obtained transfer efficiency histograms at different times after initiation of the reaction (see *SI Appendix*). Mixing the SR1-rhodanese complexes with 2 mM ATP and 2 μM GroES results in complete binding of GroES to SR1 in ~200 ms (48), which triggers the release of the substrate protein into the chaperonin cavity. Active unfolding of the substrate protein driven by the conformational changes of the apical domains of GroEL upon binding of ATP and GroES has been proposed to support protein folding (28, 49, 50). Surprisingly, we observed no obvious changes in the transfer efficiency histograms on a timescale from milliseconds to seconds (Fig. 5*B*). Only by averaging over the entire transfer efficiency histograms, we obtained a slight change in transfer efficiency of both variants by 0.05 ± 0.01 (Fig. 5*C*). The rate constant for the initial decrease of 7 ± 2 s^{-1} is close to the value reported for GroES-binding (19 s^{-1}) under these conditions (48), and the slower increase can be described with the reported rate of apical domain movement of SR1 under substrate load of 0.68 s^{-1} (48). These changes in the average transfer efficiency probably reflect very small conformational rearrangements of the substrate or the fluorophores during encapsulation, which are unlikely to be able to cause a selective deceleration of folding of the C-terminal domain inside the chaperonin cavity on the time scale of minutes to hours. We thus need to investigate alternatives for the molecular basis of the effect of the chaperonin on rhodanese folding.

Possible Contributions to the Folding Rates in the Chaperonin Cage. Changes in folding rate constants can be caused by several effects. As a starting point, we express the folding rate constant k in terms of a generalized reaction rate equation,

$$k = k_0 \exp(-\Delta G^{\ddagger}/RT) = k_0 \exp(-\Delta H^{\ddagger}/RT + \Delta S^{\ddagger}/R), \quad [1]$$

where $\Delta G^{\ddagger}$ is the height of the free-energy barrier separating the denatured from the native state, R is the gas constant, and T is the absolute temperature. The preexponential factor k_0 sets a "speed limit" (7) for the reaction and can be thought of as an attempt frequency for crossing the barrier (6).

First, we address the possibility that the decelerated folding of the C-terminal domain in the chaperonin is caused by an increase in barrier height. Since the free-energy barrier is not accessible directly, we investigate the enthalpic and entropic contributions to $\Delta G^{\ddagger}$ separately. The activation enthalpy $\Delta H^{\ddagger}$ can be obtained from the temperature dependence of the folding rate constants. Surprisingly, the rate-limiting step of rhodanese folding, i.e., folding of the N-terminal domain and formation of the native interdomain linker conformation are not affected by the chaperonin over the

---

[†]For further discussion of the effects of fluorophore labeling on the folding reaction, see *SI Appendix: Materials and Methods and Figs. S2 and S11* .
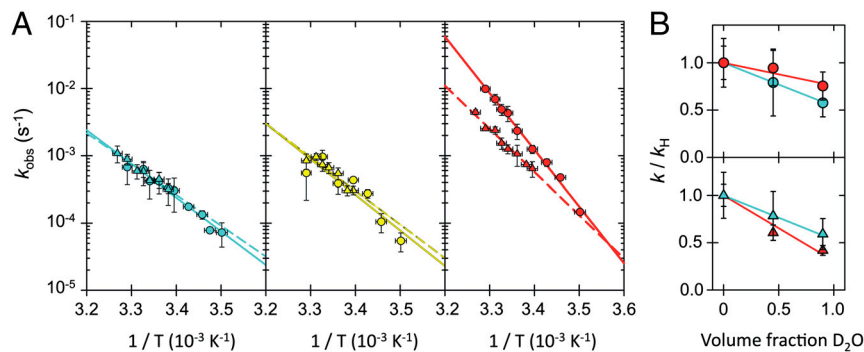
Fig. 4. Effect of temperature and solvent entropy on the autonomous and SR1-mediated folding reactions. (*A*) Arrhenius plots for the autonomous (*Circles*) and SR1-mediated (*Triangles*) folding reaction for the N variant (*Left*), L variant (Center), and C variant (*Right*). *Solid* (autonomous) and *dashed* (SR1-mediated) *lines* are Arrhenius fits according to Eq. 1. Error bars indicate standard deviations estimated from the two SVD-components or from two or three independent measurements for the cases where several measurements were available. The resulting activation enthalpies $\Delta H^{\ddagger}$ are (96 ± 7) kJ mol^{-1} (autonomous) and (88 ± 8) kJ mol^{-1} (SR1-mediated) for the N variant, (100 ± 25) kJ mol^{-1} (autonomous) and (100 ± 17) kJ mol^{-1} (SR1-mediated) for the L variant, and (161 ± 5) kJ mol^{-1} (autonomous) and (123 ± 7) kJ mol^{-1} (SR1-mediated) for the C variant. (*B*) Kinetic solvent isotope effects shown by the dependence of the ratio k/k_H on the volume fraction of D_2O at 27 °C for the autonomous (*Top*) and SR1-mediated (*Bottom*) refolding rates of the N variant (*cyan*) and C variant (*red*). Error bars indicate standard deviations estimated from at least two independent measurements, and lines represent linear regressions to illustrate the trends.
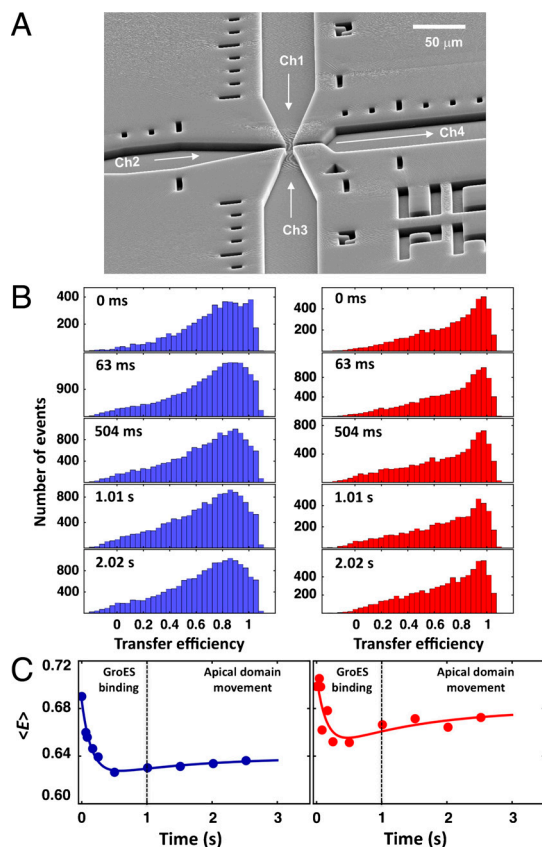
Fig. 5. Rapid processes in SR1-mediated rhodanese folding investigated with microfluidic mixing. (*A*) Scanning electron micrograph of the microfluidic mixing device (46). SR1-bound rhodanese in Ch2 is mixed with GroES and ATP in Ch1 and Ch3 in the narrow mixing region. Measurements were taken at different positions along the observation channel Ch4, corresponding to different times after mixing. (*B*) Transfer efficiency histograms of SR1-bound N variant (*Left*) and C variant (*Right*) at different times after mixing GroEL-bound rhodanese with 2 μM GroES and 2 mM ATP. (*C*) Kinetics of the average transfer efficiency ⟨E⟩ for the SR1-bound N variant (*Left*) and C variant (*Right*) obtained from the histograms in *B*. The lines represent a global double exponential fit to the data. The rate constant describing the slow increase after the initial drop was constrained to the rate constant of the apical domain movement of 0.68 s^{-1} (48). The histograms were recorded using dual excitation of donor and acceptor dyes (35, 73) to eliminate the contribution close to $E = 0$ from molecules lacking an active acceptor dye.

entire accessible temperature range (Fig. 4*A*). Assuming Arrhenius behavior, we find the activation enthalpies of the chaperonin-mediated folding reactions to be indistinguishable within experimental error from those of the autonomous reaction. However, folding of the C-terminal domain is slower in the chaperonin than free in solution at all temperatures [‡] (51), with a significantly lower activation enthalpy $(123 \pm 7 \text{ kJ mol}^{-1})$ compared to the autonomous reaction $(161 \pm 5 \text{ kJ mol}^{-1})$ (Fig. 4*A*). An increase in the enthalpic contribution to the free-energy barrier can thus be excluded as a cause of the slower folding of the C-terminal domain in the cavity.

The second possible origin of a change in $\Delta G^{\ddagger}$ is a change in activation entropy, $\Delta S^{\ddagger}$, upon encapsulation. The most important contributions to $\Delta S^{\ddagger}$ are conformational entropy and the entropy of solvation. Confinement in the chaperonin is expected to reduce the conformational entropy of the denatured state (12–16, 18). Consequently, the difference in conformational entropy of the denatured state and the transition state should decrease in the chaperonin cavity, which would reduce the height of the free-energy barrier and thus accelerate folding (12–16, 18), the opposite of what we observe. Conformational entropy is thus unlikely to be the cause of slower folding inside the chaperone.

Recent theoretical work suggests an important role of confined water molecules in chaperonin-assisted protein folding (52). We investigated this possibility by means of kinetic solvent isotope effects caused by replacing H_2O by D_2O in the samples. The stronger hydrogen bonding in D_2O is thought to increase the hydrophobic effect and stabilize proteins (53–57). If water dominated the entropy change during the chaperone-mediated folding reaction, the kinetic solvent isotope effect in the chaperone should be significantly different from that of the autonomous folding reaction. Fig. 4*B* shows the dependence of the ratio k/k_H on the volume fraction of D_2O in the buffer, where k is the refolding rate constant at different fractions of D_2O, and k_H is the rate constant in water. The rate constants for autonomous folding of both the N- and C variants of rhodanese were reduced by a factor of 1.5 to 2 in 90% D_2O. A similar decrease in the folding rate constants was found for the chaperonin-mediated folding reactions of both variants, making the presence of confined water molecules an unlikely cause of a change in folding rates in the GroEL/GroES cavity.


[‡]At temperatures above 35 °C, the GroEL/GroES-rhodanese complex tends to aggregate even at single-molecule concentrations, while at temperatures lower than 18 °C, the GroEL oligomer dissociates (51). For spontaneous rhodanese folding, the temperature range is limited by the freezing point of water at low temperature and increased quenching of the dye molecules at higher temperature, leading to poor data quality above 35 °C.

In summary, we find no indication that an increase in the free-energy barrier height is the origin of the slower folding of the C-terminal domain we observed in the chaperonin cage. Alternatively, our observation may originate from effects that essentially enter into the preexponential factor k_0 in Eq. **1**. In Kramers-type theories of protein folding (6, 58, 59), k_0 is expressed in terms of an effective intramolecular diffusion coefficient D of the polypeptide with $k_0 \propto D$, where D can be related to the roughness of the underlying free energy surface for folding (60). The reason for the lower folding rate in this picture is a decrease in the effective mobility of the polypeptide chain, which reduces the rate at which new configurations can be explored (61–63). The origin of such molecular friction can be both intra- and intermolecular interactions. For chaperonin-mediated folding, this would correspond to nonnative interactions within the folding polypeptide and interactions with the walls of the cavity.

A considerable body of theoretical work suggests that, even though moderate confinement of a polypeptide in a cavity can accelerate folding entropically, reduced folding rates are expected from stronger confinement that restricts conformational fluctuations and leads to an increase in molecular friction (13–19). In view of the small size of the chaperonin cavity, resembling a sphere with a radius of ~3 nm (assuming a cavity volume of 120 nm^3 (64)), compared to the radius of gyration of denatured rhodanese of ~3.8 nm (calculated assuming the typical persistence length of 0.4 nm for unfolded protein chains under native conditions (65)), a significant effect of confinement on the folding dynamics of rhodanese may be expected. However, confinement alone should influence the folding rates of both domains to a similar extent, in contrast to our experimental observation, implying an additional influence of interactions of the substrate with the cavity walls (20, 31). Recent theoretical work indicates a pronounced effect of the interaction strength between cage and protein on folding rates: moderate interaction strengths can, in a narrow range, accelerate folding by iterative binding and dissociation events, but simulations predict a deceleration of folding for strong interactions (11, 16, 66). Evidence for such interactions comes from our microfluidic mixing experiments (Fig. 5*B*), which indicate a lack of conformational rearrangements of rhodanese during encapsulation, and thus suggest that interactions between rhodanese and GroEL persist in the encapsulated state. Even the first histograms from the manual mixing experiments (Fig. 2*A*) still resemble those of the binary SR1-rhodanese complex (Fig. 1*B*). Recent cryoelectron microscopy experiments show that substrate proteins bound to GroEL are predominantly localized deep inside the cavity (67, 68), a situation that will facilitate interactions with the chaperonin walls in the GroEL-bound state. The particularly strong interactions of rhodanese with GroEL (69, 70) are thus likely to increase molecular friction of the substrate protein in the cavity. If we assume that the effect of such interactions can be approximated by an effective dissociation step from the chaperonin wall, protein-chaperone interactions will become rate-limiting for faster processes, such as folding of the C-terminal domain, whereas slower processes, such as folding of the N-terminal domain, will be much less affected, in agreement with our observations (Fig. 6). A further understanding of the molecular basis of these effects will benefit greatly from the increasingly detailed information available from theory and simulations (20).

Our results illustrate how multiparameter single-molecule spectroscopy in combination with microfluidic mixing opens a new opportunity for identifying previously elusive effects of molecular chaperones on protein folding mechanisms. Major advantages of the approach are the availability of distributions of observables instead of mean values, the complementarity of the different types of spectroscopic information from a single measurement that can be used for a global analysis of all observables, the broad range of time scales accessible, and the extremely low protein concentrations employed, which allow aggregation to
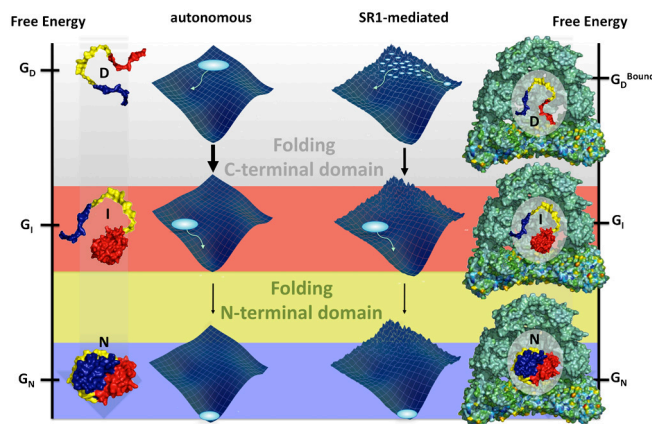
Fig. 6. Schematic of the autonomous and SR1-mediated folding of rhodanese. Rhodanese folds via a partially folded intermediate, in which the C-terminal domain (*red*) is already folded (*Left*). In the chaperonin-mediated reaction, molecular friction (energetic roughness) from interactions with the cavity wall decelerates the folding of the C-terminal domain. However, the folding pathway of rhodanese is preserved (*Right*).

be excluded from affecting the folding kinetics. Although the biological function of the GroEL/GroES system is suggestive of an acceleration of folding rates, our results show that chaperonins can even slow down protein folding processes, and support the view that preventing aggregation of proteins is more important for cellular viability than accelerating protein folding reactions (71). However, our observations call for a differentiated view of chaperone action: since the folding rates of the domains within a single protein can be affected differently by the chaperonin, it is improbable that there is one universal chaperonin mechanism at work. This notion is supported by the large variability of effects of chaperonins on the folding of different proteins reported in the literature (20) and by theoretical concepts that provide a quantitative framework for the competition between intra- and intermolecular interactions that determine the folding rate and mechanism of a substrate protein inside the GroEL/GroES cage (1, 8, 11–20, 66). Future experimental and theoretical investigations will have to address the potential synergies of the different mechanisms, whose subtle balance may be required to achieve the promiscuity of many molecular chaperones.

Materials and Methods

1. Thirumalai D, Lorimer GH (2001) Chaperonin-mediated protein folding. *Annu Rev Biophys Biomol Struct* 30:245–269.
2. Hartl FU, Hayer-Hartl M (2002) Protein folding—Molecular chaperones in the cytosol: from nascent chain to folded protein. *Science* 295:1852–1858.
3. Bukau B, Weissman J, Horwich A (2006) Molecular chaperones and protein quality control. *Cell* 125:443–451.
4. Ellgaard L, Helenius A (2003) Quality control in the endoplasmic reticulum. *Nat Rev Mol Cell Biol* 4:181–191.
5. Fersht AR (1998) *Structure and mechanism in protein science* (W.H. Freeman and Company, New York).
6. Bryngelson JD, Onuchic JN, Socci ND, Wolynes PG (1995) Funnels, pathways, and the energy landscape of protein folding: a synthesis. *Proteins* 21:167–195.
7. Eaton WA, et al. (2000) Fast kinetics and mechanisms in protein folding. *Annu Rev Biophys Biomol Struct* 29:327–359.
8. Thirumalai D, O'Brien EP, Morrison G, Hyeon C (2010) Theoretical perspectives on protein folding. *Annu Rev Biophys* 39:159–183.
9. Fenton WA, Horwich AL (2003) Chaperonin-mediated protein folding: fate of substrate polypeptide. *Quarterly Reviews of Biophysics* 36:229–256.
10. Apetri AC, Horwich AL (2008) Chaperonin chamber accelerates protein folding through passive action of preventing aggregation. *Proc Natl Acad Sci USA* 105:17351–17355.
11. Betancourt MR, Thirumalai D (1999) Exploring the kinetic requirements for enhancement of protein folding rates in the GroEL cavity. *J Mol Biol* 287:627–644.
12. Zhou HX, Dill KA (2001) Stabilization of proteins in confined spaces. *Biochemistry* 40:11289–11293.
13. Klimov DK, Newfield D, Thirumalai D (2002) Simulations of beta-hairpin folding confined to spherical pores using distributed computing. *Proc Natl Acad Sci USA* 99:8019–8024.
14. Baumketner A, Jewett A, Shea JE (2003) Effects of confinement in chaperonin assisted protein folding: rate enhancement by decreasing the roughness of the folding energy landscape. *J Mol Biol* 332:701–713.
15. Takagi F, Koga N, Takada S (2003) How protein thermodynamics and folding mechanisms are altered by the chaperonin cage: molecular simulations. *Proc Natl Acad Sci USA* 100:11367–11372.
16. Jewett AI, Baumketner A, Shea JE (2004) Accelerated folding in the weak hydrophobic environment of a chaperonin cavity: creation of an alternate fast folding pathway. *Proc Natl Acad Sci USA* 101:13192–13197.
17. Cheung MS, Klimov D, Thirumalai D (2005) Molecular crowding enhances native state stability and refolding rates of globular proteins. *Proc Natl Acad Sci USA* 102:4753–4758.
18. Mittal J, Best RB (2008) Thermodynamics and kinetics of protein folding under confinement. *Proc Natl Acad Sci USA* 105:20233–20238.
19. Zhou HX (2008) Protein folding in confined and crowded environments. *Arch Biochem Biophys* 469:76–82.
20. Jewett A, Shea J (2009) Reconciling theories of chaperonin accelerated folding with experimental evidence. *Cell Mol Life Sci* 67:255–276.
21. Schuler B, Eaton WA (2008) Protein folding studied by single-molecule FRET. *Curr Opin Struct Biol* 18:16–26.
22. Michalet X, Weiss S, Jäger M (2006) Single-molecule fluorescence studies of protein folding and conformational dynamics. *Chem Rev* 106:1785–1813.
23. Borgia A, Williams P, Clarke J (2008) Single-molecule studies of protein folding. *Annu Rev Biochem* 77:101–125.
24. Haran G (2003) Single-molecule fluorescence spectroscopy of biomolecular folding. *J Phys Cond Mat* 15:R1291–R1317.
25. Yamasaki R, et al. (1999) Single molecular observation of the interaction of GroEL with substrate proteins. *J Mol Biol* 292:965–972.
26. Taguchi H, Ueno T, Tadakuma H, Yoshida M, Funatsu T (2001) Single-molecule observation of protein-protein interactions in the chaperonin system. *Nat Biotechnol* 19:861–865.
27. Hillger F, et al. (2008) Probing protein-chaperone interactions with single-molecule fluorescence spectroscopy. *Angewandte Chemie International Edition* 47:6184–6188.
28. Sharma S, et al. (2008) Monitoring protein conformation along the pathway of chaperonin-assisted folding. *Cell* 133:142–153.
29. Frank GA, et al. (2010) Out-of-equilibrium conformational cycling of GroEL under saturating ATP concentrations. *Proc Natl Acad Sci USA* 107:6270–6274.
30. Mickler M, Hessling M, Ratzke C, Buchner J, Hugel T (2009) The large conformational changes of Hsp90 are only weakly coupled to ATP hydrolysis. *Nat Struct Mol Biol* 16:281–286.
31. Tang YC, et al. (2006) Structural features of the GroEL-GroES nano-cage required for rapid folding of encapsulated protein. *Cell* 125:903–914.
32. Farr GW, Fenton WA, Horwich AL (2007) Perturbed ATPase activity and not "close confinement" of substrate in the *cis* cavity affects rates of folding by tail-multiplied GroEL. *Proc Natl Acad Sci USA* 104:5342–5347.
33. Mendoza JA, Rogers E, Lorimer GH, Horowitz PM (1991) Chaperonins facilitate the in vitro folding of monomeric mitochondrial rhodanese. *J Biol Chem* 266:13044–13049.
34. Widengren J, et al. (2006) Single-molecule detection and identification of multiple species by multiparameter fluorescence detection. *Anal Chem* 78:2039–2050.
35. Kapanidis AN, et al. (2004) Fluorescence-aided molecule sorting: analysis of structure and interactions by alternating-laser excitation of single molecules. *Proc Natl Acad Sci USA* 101:8936–8941.
36. Müller BK, Zaychikov E, Bräuchle C, Lamb DC (2005) Pulsed interleaved excitation. *Biophys J* 89:3508–3522.
37. Weissman JS, Rye HS, Fenton WA, Beechem JM, Horwich AL (1996) Characterization of the active intermediate of a GroEL-GroES-mediated protein folding reaction. *Cell* 84:481–490.
38. Weissman JS, et al. (1995) Mechanism of GroEL action: productive release of polypeptide from a sequestered position under GroES. *Cell* 83:577–587.
39. Henry E, Hofrichter J (1992) Singular value decomposition—Application to analysis of experimental data. *Methods Enzymol* 210:129–192.
40. Doose S, Neuweiler H, Sauer M (2009) Fluorescence quenching by photoinduced electron transfer: a reporter for conformational dynamics of macromolecules. *Chemphyschem* 10:1389–1398.
41. Brinker A, et al. (2001) Dual function of protein confinement in chaperonin-assisted protein folding. *Cell* 107:223–233.
42. Chaudhry C, et al. (2003) Role of the gamma-phosphate of ATP in triggering protein folding by GroEL-GroES: function, structure and energetics. *EMBO J* 22:4877–4887.
43. Hillger F, Nettels D, Dorsch S, Schuler B (2007) Detection and analysis of protein aggregation with confocal single molecule fluorescence spectroscopy. *J Fluoresc* 17:759–765.
44. Lipman EA, Schuler B, Bakajin O, Eaton WA (2003) Single-molecule measurement of protein folding kinetics. *Science* 301:1233–1235.
45. Nguyen NT, Wu ZG (2005) Micromixers—a review. *J Micromech Microeng* 15:R1–R16.
46. Pfeil SH, Wickersham CE, Hoffmann A, Lipman EA (2009) A microfluidic mixing system for single-molecule measurements. *Rev Sci Instrum* 80:055105.
47. Lemke EA, et al. (2009) Microfluidic device for single-molecule experiments with enhanced photostability. *J Am Chem Soc* 131:13610–13612.
48. Motojima F, Chaudhry C, Fenton WA, Farr GW, Horwich AL (2004) Substrate polypeptide presents a load on the apical domains of the chaperonin GroEL. *Proc Natl Acad Sci USA* 101:15005–15012.
49. Lin Z, Madan D, Rye HS (2008) GroEL stimulates protein folding through forced unfolding. *Nat Struct Mol Biol* 15:303–311.
50. Shtilerman M, Lorimer GH, Englander SW (1999) Chaperonin function: folding by forced unfolding. *Science* 284:822–825.
51. Panda M, Horowitz PM (2004) Activation parameters for the spontaneous and pressure-induced phases of the dissociation of single-ring GroEL (SR1) chaperonin. *Protein J* 23:85–94.
52. England J, Lucent D, Pande V (2008) Rattling the cage: computational models of chaperonin-mediated protein folding. *Curr Opin Struct Biol* 18:163–169.
53. Kresheck GC, Schneider H, Scheraga HA (1965) The effect of D$_2$O on the thermal stability of proteins. Thermodynamic parameters for the transfer of model compounds from H$_2$O to D$_2$O. *J Phys Chem* 69:3132–3144.
54. Makhatadze GI, Clore GM, Gronenborn AM (1995) Solvent isotope effect and protein stability. *Nat Struct Biol* 2:852–855.
55. Parker MJ, Clarke AR (1997) Amide backbone and water-related H/D isotope effects on the dynamics of a protein folding reaction. *Biochemistry* 36:5786–5794.
56. Lopez MM, Makhatadze GI (1998) Solvent isotope effect on thermodynamics of hydration. *Biophys Chem* 74:117–125.
57. Dougan L, Koti AS, Genchev G, Lu H, Fernandez JM (2008) A single-molecule perspective on the role of solvent hydrogen bonds in protein folding and chemical reactions. *Chemphyschem* 9:2836–2847.
58. Kramers H (1940) Brownian motion in a field of force and the diffusion model of chemical reactions. *Physica* 7:284–304.
59. Socci ND, Onuchic JN, Wolynes PG (1996) Diffusive dynamics of the reaction coordinate for protein folding funnels. *J Chem Phys* 104:5860–5868.
60. Zwanzig R (1988) Diffusion in a rough potential. *Proc Natl Acad Sci USA* 85:2029–2030.
61. Möglich A, Joder K, Kiefhaber T (2006) End-to-end distance distributions and intrachain diffusion constants in unfolded polypeptide chains indicate intramolecular hydrogen bond formation. *Proc Natl Acad Sci USA* 103:12394–12399.
62. Nettels D, Gopich IV, Hoffmann A, Schuler B (2007) Ultrafast dynamics of protein collapse from single-molecule photon statistics. *Proc Natl Acad Sci USA* 104:2655–2660.
63. Cellmer T, Henry E, Hofrichter J, Eaton W (2008) Measuring internal friction of an ultrafast-folding protein. *Proc Natl Acad Sci USA* 47:18320–18325.
64. Horwich AL, Farr GW, Fenton WA (2006) GroEL-GroES-mediated protein folding. *Chem Rev* 106:1917–1930.
65. Zhou HX (2004) Polymer models of protein stability, folding, and interactions. *Biochemistry* 43:2141–2154.
66. Cheung MS, Thirumalai D (2006) Nanopore-protein interactions dramatically alter stability and yield of the native state in restricted spaces. *J Mol Biol* 357:632–643.
67. Elad N, et al. (2007) Topologies of a substrate protein bound to the chaperonin GroEL. *Mol Cell* 26:415–426.
68. Clare DK, Bakkes PJ, van Heerikhuizen H, van der Vies SM, Saibil HR (2009) Chaperonin complex with a newly folded protein encapsulated in the folding chamber. *Nature* 457:107–110.
69. Mayhew M, et al. (1996) Protein folding in the central cavity of the GroEL-GroES chaperonin complex. *Nature* 379:420–426.
70. Martin J, Hartl FU (1997) The effect of macromolecular crowding on chaperonin-mediated protein folding. *Proc Natl Acad Sci USA* 94:1107–1112.
71. Ellis RJ (2001) Molecular chaperones: inside and outside the Anfinsen cage. *Curr Biol* 11:R1038–1040.
72. Horwich AL, Burston SG, Rye HS, Weissman JS, Fenton WA (1998) Construction of single-ring and two-ring hybrid versions of bacterial chaperonin GroEL. *Methods Enzymol* 290:114–116.
73. Müller BK, Zaychikov E, Bräuchle C, Lamb DC (2005) Pulsed interleaved excitation. *Biophys J* 89:3508–3522.

Supporting information Hofmann *et al.*

Materials and Methods

Protein preparation. GroES was expressed in BL21DE3 cells. After cell disruption in 50 mM TrisHCl, 1 mM EDTA, pH 7.5 (buffer A) and centrifugation for 15 min at 4 °C (21000 rpm, F21S50 rotor, Herolab), the supernatant was filtered and loaded on a Q-sepharose column (GE Healthcare Biosciences, Piscataway, NJ) equilibrated with buffer A (1). The column was washed with 500 ml of buffer A before starting a gradient from 0 to 1 M NaCl at a flow rate of 4 ml/min. Fractions containing GroES were combined. After heat precipitation for 20 min at 80°C in the presence of 10 mM EDTA (2), GroES was 80 % pure (according to SDS-PAGE). The remaining impurities were removed by size exclusion chromatography (Sephadex S75 26/60, GE Healthcare Biosciences, Piscataway, NJ) under denaturing conditions (50 mM TrisHCl, 1.5 M GdmCl, 1 mM EDTA, pH 7.5). Finally, the protein was refolded by dialyzing twice against 1 liter of buffer A, frozen in liquid nitrogen, and stored at -80°C. GroEL-SR1 was expressed and purified essentially as described by Horwich *et al.* (3) and stored at -80 °C as a precipitate in 2.7 M ammonium sulfate. Cysteine variants of rhodanese (E77C, D102C, K135C, K174C, D219C, K236C, E285C, E77C/K135C, K135C/K174C, K236C/E285C) were prepared and labeled with Alexa Fluor 488 and Alexa Fluor 594 (Förster radius of 5.4 nm (4-6)) as described previously (6).

We have taken the following measures to minimize the risk of perturbing the refolding kinetics by fluorophore labeling. [1] We selected chromophores with good solubility in water, which showed little or no influence on protein stability and dynamics in previous experiments (4, 7-12). [2] Previous size exclusion chromatography experiments showed no binding of the free dyes, labeled peptides, and small proteins to GroEL (6). Considering the very tight binding of rhodanese to GroEL, it seems improbable that the fluorophores have a strong effect on the interactions with the chaperone. [3] The remarkable promiscuity of GroEL/ES for different substrate proteins suggests that the chaperone will not be particularly sensitive to protein modifications. [4] We are directly comparing the folding kinetics of identically labeled proteins in free solution and inside the chaperonin cage.

Preparation of rhodanese-chaperone complexes. The ammonium sulfate precipitate of SR1 was resolubilized at 1 µM SR1 (heptamer) in folding buffer (50 mM TrisHCl (Roth), 10 mM MgCl$_2$ (Roth), 5 mM KCl (Roth), 100 mM 2-mercaptoethanol (Fluka Ultra), 0.001 % Tween 20 (Pierce), pH 7.5). Binding of rhodanese to SR1 was achieved by manually mixing 10 µl of 0.6 to 2 µM Rhodanese unfolded in 5 M GdmCl, 50 mM TrisHCl, 10 mM MgCl$_2$, 5 mM KCl, 100 mM 2-mercaptoethanol, 0.001 % Tween 20, pH 7.5 with 190 µl of a 1 µM solution of SR1 (heptamer). The complex was purified by size exclusion chromatography on a TSK 5000 PWXL column (TOSOH Bioscience) using fluorescence

detection. In the presence of 1 μM GroES and 2 mM ATP, the complexes of SR1-encapsulated rhodanese were stable for more than 100 min (Fig. S1).

Refolding experiments by manual mixing. Binary complexes of SR1 and rhodanese were prepared as described above. Chaperone-mediated refolding experiments were performed in folding buffer; they were initiated by the addition of GroES (final concentration 1 μM) and ATP (final concentration of 2 mM) to the SR1-rhodanese complexes. The spontaneous refolding reaction was observed by diluting rhodanese unfolded in 4 M GdmCl 100-fold into folding buffer. For experiments at different volume fractions of D_2O, the SR1-rhodanese complexes and unfolded rhodanese were incubated in folding buffer at the respective D_2O/H_2O mixture for 1 h before refolding was initiated. All solvent isotope exchange experiments were performed at 27 °C.

Fluorescence anisotropy measurements. Steady-state fluorescence anisotropy measurements were performed in folding buffer in a Fluorolog 3 fluorometer (HORIBA Jobin Yvon, Germany). Native encapsulated rhodanese was prepared by incubating the purified binary SR1-rhodanese complexes (size exclusion chromatography, PWXL column, TOSOH Bioscience) for 1h with 2 mM ATP and 1 μM GroES. The excitation and emission wavelengths were 488 nm and 515 nm for donor and 590 nm and 615 nm for acceptor anisotropy measurements, respectively. The excitation and emission slits were 5 nm, and an integration time of 1 s was used. In total, 60 data points were measured, and an average anisotropy was calculated from these values (Fig. S2).

Reactivation of rhodanese using an enzymatic assay (13). Binary complexes of SR1 with the L-variant of rhodanese were prepared by incubating 2 μM SR1 with 1 μM donor- and acceptor-labeled rhodanese in 50 μl folding buffer for 2h at 37°C. The binary complex was purified by size exclusion chromatography on a TSK 5000 PWXL column (TOSOH Bioscience). The concentration of rhodanese in this binary complex was 0.1 μM (according to the fluorescence of Alexa Fluor 594) in 500 μl folding buffer. A premix containing 0.05 M KCN, 0.04 M KH_2PO_4, and 0.05 M $Na_2S_2O_3$ was prepared. To trigger refolding, 2 mM ATP and 1 μM GroES were added to 100 μl of binary complex (27°C). After different times (0, 10, 15, 20, 25, 30, 40, 60, 80 min), 10 μl of the reaction were mixed with 1 μl of 0.5 M EDTA (pH7.3) and cooled on ice. 125 μl of the premix were added to the mixture, and the enzymatic reaction was allowed to proceed for 1 minute before stopping it by the addition of 62.5 μl 15% formaldehyde. To detect the product, SCN^-, 187.5 μl of a 6 % (w/v) $Fe(NO_3)_3$ solution in 12 % HNO_3 were added. The complexes of iron(III) with SCN^- were detected by their absorbance at 460 nm. Three independent replicates were used to determine the rate constant for reactivation (Fig. S11). Because of the very low rhodanese concentrations used in this experiment, a background reaction due to spontaneous refolding

of rhodanese during the dissociation of the complex on ice occurred. The background reaction was accounted for by repeating the reaction without the addition of GroES and ATP and subtracting it from the data. A single-exponential fit of the corrected data yielded a rate constant of 0.09 ± 0.04 min^{-1} (Fig. S11), within the range of rate constants (from ~0.04 min^{-1} to ~0.16 min^{-1}) reported in the literature for unlabeled rhodanese (14-17).

Limited proteolysis assay. Two singly-donor labeled variants (K135C-D and E285C-D) were used for limited proteolysis to probe the sequence of folding events in rhodanese (Fig. S10). Position K135C is located at the N-terminal end of the linker connecting the N- and C-terminal domains, whereas E285C is located in the C-terminal domain. The unfolded rhodanese variants (14 µM K135C-D and 7 µM E285C-D in 4 M GdmCl and folding buffer) were diluted (1:10) with folding buffer to a final volume of 200 µl. 100 seconds after starting the refolding reaction, 20 µl of a 20 mg/ml stock-solution of proteinase K were added. Proteolysis was stopped by mixing an aliquot of the reaction mixture (100 µl) with 10 µl 120% w/v TCA at 100 s and 300s after protease addition. The precipitate was dissolved in 50 µl SDS PAGE loading-buffer, and 10 µl were used for electrophoresis. The fluorescence of the attached Alexa Fluor 488 was measured in the gel (Fig. S10B) before staining with Coomassie brilliant blue R250 (Roth, Karlsruhe, Germany) (Fig. S10A). The fluorescence image (Fig. S10B, excitation wavelength 488 nm; Typhoon 9400, Amersham) shows a band with a mass of approximately 11 kD for variant E285C-D (fluorophore in the C-terminal domain), whereas only smaller fragments are observed for K135C-D (fluorophore in the N-terminal domain), suggesting that the C-terminal domain folds prior to the N-terminal domain. The molecular mass of the C-terminal domain (starting with Y163) is estimated to be 14 851 Da. Due to the high amount of protease used in the assay (2 mg/ml), no band of undigested rhodanese could be observed.

Single molecule measurements. Observations of single-molecule fluorescence were made using a MicroTime 200 confocal microscope (PicoQuant, Berlin, Germany) equipped with a 488 nm diode laser (Sapphire 488-100 CDRH, Coherent, Santa Clara, CA), a 80 MHz-pulsed laser (Optical Supercontinuum System SCF450-4-80MHz, Fianium, Southampton, UK), a 30 MHz-pulsed laser (Optical Supercontinuum System SCF450-4-30MHz Fianium), and an Olympus UplanApo 60x/1.20W objective. After passing through a 100 µm pinhole, sample fluorescence was separated first into parallel and perpendicular polarized light relative to the polarization of the exciting laser beam using a polarizing beam splitter cube. Afterwards, the two components were further separated into donor and acceptor components using a dichroic mirror (585DCXR, Chroma, Rockingham, VT). After passing two filters (Chroma ET525/50M, HQ650/100), each component was focused onto an avalanche photodiode (SPCM-AQR-15, PerkinElmer Optoelectronics, Vaudreuil, QC, Canada), and the arrival time of every detected photon was recorded using a

HydraHarp 400 counting card (PicoQuant, Berlin, Germany). All measurements were performed with laser powers of 70 µW to 100 µW. For dual color excitation of donor and acceptor (18, 19), the donor was excited continuously with a 488 nm diode laser (Sapphire 488-100 CDRH, Coherent, Santa Clara, CA) to maximize the excitation rate, and the acceptor was excited with picosecond pulses at a wavelength range selected by a z582/15 (Chroma) band pass filter and a pulse frequency of 30 MHz (Optical Supercontinuum Systems SCF450-4-30MHz Fianium, Southampton, UK). Successive photons detected in either channel and separated by less than 130 µs were combined into one burst. A burst was retained as a significant event if the total number of counts exceeded 20 (or 15 in case of the N-variant in the microfluidic mixer). Identified bursts were corrected for background, differences in quantum yields of donor and acceptor, the different collection efficiencies in the detection channels, cross-talk, and direct acceptor excitation as described previously (20). In addition, bursts during which acceptor photobleaching is likely to have occurred were discarded (6). A custom-built temperature-controlled sample holder employing peltier elements and a digital temperature controller (TC2812-LAB12, Cooltronic, Wil, Switzerland) with a PT100 platinum resistance temperature sensor (Minco EC AG, Wil, Switzerland) was used to adjust the temperature (21). The temperature in the confocal volume was determined via the temperature-dependent fluorescence lifetime of rhodamine B (RhB) (22) measured in a custom-built temperature-controlled ensemble time-correlated single photon counting instrument (23).

Data reduction by moving window analysis and singular value decomposition (SVD).
For the moving window analysis, window sizes of $\Delta t = 300$ s (spontaneous folding of the N- and L-variant and SR1-mediated folding of N-, L-, and C-variant) or $\Delta t = 50$ s (spontaneous folding of the C-variant) were used. All bursts recorded within this window were used to obtain the following nine observables: transfer efficiency, burst duration, photon rate per burst (photon detection rate), donor fluorescence lifetime (parallel and perpendicular relative to the polarization of the excitation light), acceptor fluorescence lifetime (parallel and perpendicular to the polarization of the excitation light), donor anisotropy after donor excitation, and acceptor anisotropy after donor excitation. The observables were binned (25x25 bins) in two-dimensional histograms, with the transfer efficiency as one dimension. Bin-ranges were from $E_{min} = -0.3$ to $E_{max} = 1.2$ (transfer efficiency), $t_{min} = 0$ ms to $t_{max} = 10$ ms (burst duration), $B_{min} = 0$ ms^{-1} to $B_{max} = 100$ ms^{-1} (photon detection rate), $r_{min} = -2$ to $r_{max} = 2$ (anisotropy), and $\tau_{min} = 0$ ns to $\tau_{max} = 8$ ns (fluorescence lifetime). Every 2D-histogram was expressed column by column as a vector $\mathbf{a}_i(t_1)$ with 625 elements (25x25) for the first time window t_1. By arranging all sub-vectors $\mathbf{a}_i(t_1)$ in one vector $\mathbf{a}(t_1) = [\mathbf{a}_1(t_1), \mathbf{a}_2(t_1), \mathbf{a}_3(t_1),…, \mathbf{a}_8(t_1)]$, the final vector (containing 5000 elements) for this time window (t_1) was obtained. The window was then shifted incrementally by $\Delta t/3$, and $\mathbf{a}(t_j)$ was calculated for the bursts resulting from every window

position. For the SVD, a time $t = t_s + \Delta t/2$ was assigned to every histogram, where t_s is the start time of the corresponding window. The procedure yields an $m \times n$ data matrix, **A**, with n vectors $\mathbf{a}(t_j)$ for n time points and $m = 5000$ bins of the nine observables.

SVD decomposes **A** into three matrices (**U**, **S** and **V**) (24):

$$\mathbf{A} = \mathbf{U}\,\mathbf{S}\,\mathbf{V^T}. \qquad\qquad\qquad [S1]$$

Here, **U** is an $m \times m$ matrix of basis vectors (eigenvectors of $\mathbf{AA^T}$), **S** is an $m \times n$ rectangular diagonal matrix whose elements give the weighting factors (or singular values) for every basis vector (the squared eigenvalues of $\mathbf{AA^T}$ and $\mathbf{A^TA}$), and $\mathbf{V^T}$ is a transposed $n \times n$ matrix of amplitude vectors (eigenvectors of $\mathbf{A^TA}$), describing the time course of the corresponding basis vectors. The number of nonzero diagonal elements of **S** that are necessary to reconstruct the data matrix from **U**, **S,** and **V** is an estimate of the number of distinguishable molecular species involved in the reaction mechanism. The two-dimensional representations of the first three basis vectors and the first three amplitude vectors for the spontaneous and SR1-mediated folding reaction of the N-variant, L-variant and C-variant are shown in Fig. S6, S7, S8 and S9, respectively. Raw data showing the first histograms immediately after starting the refolding reaction and the last histogram of the refolding reaction are shown for all three variants in Figs. S3, S4 and S5.

Microfluidic mixing experiments. For rapid mixing experiments, microfluidic mixers fabricated by replica molding in polydimethylsiloxane (PDMS) were used. For detecting the GroES-ATP-mediated encapsulation reaction of the SR1-bound rhodanese variants, the binary rhodanese-SR1 complex was mixed at a ratio of 1:5.7 with 2.4 µM GroES and 2.4 mM ATP, resulting in final concentrations of 2 µM GroES and 2 mM ATP. 0.01 % Tween 20 were included to prevent non-specific interactions of the chaperone-substrate complexes with the PDMS surfaces. Measurements were taken by placing the confocal volume at positions 75 µm (63 ms), 100 µm (94 ms), 200 µm (168 ms), 300 µm (252 ms), 600 µm (504 ms and 1.01 s), 900 µm (1.51 s), 1200 µm (2.02 s), and 1500 µm (2.52 s) downstream of the mixing region. To determine the transfer efficiency histogram at $t = 0$, the binary rhodanese-chaperone complex was measured 50 µm after the mixing region, without ATP and GroES in the side channels (Ch1 and Ch3, see Fig. 5A). The experiments were performed with pressures of 13.8 kPa (2.0 psi) applied to all channels for measurements from 50 µm (without GroES and ATP, 0 ms) to 600 µm (504 ms), and with 6.9 kPa (1.0 psi) for all measurements from 600 µm (1.01 s) to 1500 µm (2.52 s). The calculated flow velocities of 1.2 mm/s (13.8 kPa) and 0.6 mm/s (6.9 kPa) in the observation channel (Ch4) were used to convert distances to times as described by Pfeil *et al*. (25). The calculated velocities were confirmed by analyzing the donor-acceptor fluorescence intensity cross-correlation functions (26).

References

1. Quaite-Randall E & Joachimiak A (2000) Purification of GroES from an Overproducing E.coli Strain. *Methods Mol Biol* 140:41-49.
2. Kamireddi M, Eisenstein E, & Reddy P (1997) Stable expression and rapid purification of Escherichia coli GroEL and GroES chaperonins. *Protein Expr Purif* 11:47-52.
3. Horwich AL, Burston SG, Rye HS, Weissman JS, & Fenton WA (1998) Construction of single-ring and two-ring hybrid versions of bacterial chaperonin GroEL. *Methods Enzymol* 290:114-116.
4. Hoffmann A, Kane A, Nettels D, Hertzog DE, Baumgärtel P*, et al.* (2007) Mapping protein collapse with single-molecule fluorescence and kinetic synchrotron radiation circular dichroism spectroscopy. *Proc Natl Acad Sci USA* 104:105-110.
5. Nettels D, Gopich IV, Hoffmann A, & Schuler B (2007) Ultrafast dynamics of protein collapse from single-molecule photon statistics. *Proc Natl Acad Sci USA* 104:2655-2660.
6. Hillger F, Hänni D, Nettels D, Geister S, Grandin M*, et al.* (2008) Probing protein-chaperone interactions with single-molecule fluorescence spectroscopy. *Angew Chem Int Ed* 47:6184-6188.
7. Schuler B, Lipman EA, & Eaton WA (2002) Probing the free-energy surface for protein folding with single-molecule fluorescence spectroscopy. *Nature* 419:743-747.
8. Sherman E & Haran G (2006) Coil-globule transition in the denatured state of a small protein. *Proc Natl Acad Sci USA* 103:11539-11543.
9. Hofmann H, Golbik RP, Ott M, Hübner CG, & Ulbrich-Hofmann R (2008) Coulomb forces control the density of the collapsed unfolded state of barstar. *J Mol Biol* 376:597-605.
10. Tezuka-Kawakami T, Gell C, Brockwell DJ, Radford SE, & Smith DA (2006) Urea-induced unfolding of the immunity protein Im9 monitored by spFRET. *Biophys. J.* 91:L42-L44.
11. Merchant KA, Best RB, Louis JM, Gopich IV, & Eaton WA (2007) Characterizing the unfolded states of proteins using single-molecule FRET spectroscopy and molecular simulations. *Proc Natl Acad Sci USA* 104:1528-1533.
12. Margittai M, Widengren J, Schweinberger E, Schroder GF, Felekyan S*, et al.* (2003) Single-molecule fluorescence resonance energy transfer reveals a dynamic equilibrium between closed and open conformations of syntaxin 1. *Proc Natl Acad Sci USA* 100:15516-15521.
13. Tandon S & Horowitz PM (1989) Reversible folding of rhodanese. Presence of intermediate(s) at equilibrium. *J Biol Chem* 264:9859-9866.
14. Chaudhry C, Farr GW, Todd MJ, Rye HS, Brunger AT*, et al.* (2003) Role of the gamma-phosphate of ATP in triggering protein folding by GroEL-GroES: function, structure and energetics. *EMBO J* 22:4877-4887.
15. Weissman JS, Rye HS, Fenton WA, Beechem JM, & Horwich AL (1996) Characterization of the active intermediate of a GroEL-GroES-mediated protein folding reaction. *Cell* 84:481-490.
16. Tang Y, Chang H, Chakraborty K, Hartl F, & Hayer-Hartl M (2008) Essential role of the chaperonin folding compartment in vivo. *EMBO J.*

17. Farr GW, Fenton WA, & Horwich AL (2007) Perturbed ATPase activity and not "close confinement" of substrate in the cis cavity affects rates of folding by tail-multiplied GroEL. *Proc Natl Acad Sci USA* 104:5342-5347.
18. Müller BK, Zaychikov E, Bräuchle C, & Lamb DC (2005) Pulsed interleaved excitation. *Biophys. J.* 89:3508-3522.
19. Kapanidis AN, Lee NK, Laurence TA, Doose S, Margeat E*, et al.* (2004) Fluorescence-aided molecule sorting: analysis of structure and interactions by alternating-laser excitation of single molecules. *Proc Natl Acad Sci USA* 101:8936-8941.
20. Schuler B (2007) Application of single molecule Förster resonance energy transfer to protein folding. *Methods Mol Biol* 350:115-138.
21. Nettels D, Müller-Späth S, Küster F, Hofmann H, Haenni D*, et al.* (2009) Single-molecule spectroscopy of the temperature-induced collapse of unfolded proteins. *Proc Natl Acad Sci USA*.
22. Benninger RK, Koç Y, Hofmann O, Requejo-Isidro J, Neil MA*, et al.* (2006) Quantitative 3D mapping of fluidic temperatures within microchannel networks using fluorescence lifetime imaging. *Anal Chem* 78:2272-2278.
23. Nettels D, Hoffmann A, & Schuler B (2008) Unfolded Protein and Peptide Dynamics Investigated with Single-Molecule FRET and Correlation Spectroscopy from Picoseconds to Seconds. *J Phys Chem B*.
24. Henry E & Hofrichter J (1992) Singular value decomposition - Application to analysis of experimental data. *Methods Enzymol* 210:129-192.
25. Pfeil SH, Wickersham CE, Hoffmann A, & Lipman EA (2009) A microfluidic mixing system for single-molecule measurements. *Rev Sci Instrum* 80:055105.
26. Gösch M, Blom H, Holm J, & Rigler R (2000) Hydrodynamic flow profiling in microchannel structures by single molecule fluorescence spectroscopy. *Anal Chem* 72:3260-3265.
27. Hillger F, Nettels D, Dorsch S, & Schuler B (2007) Detection and analysis of protein aggregation with confocal single molecule fluorescence spectroscopy. *J Fluoresc* 17:759-765.

Supporting Figures
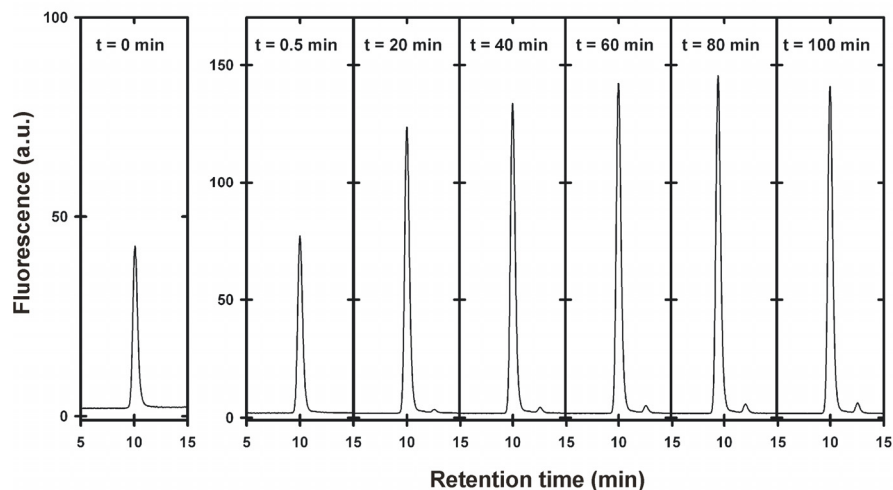
Fig. S1. Stability of the SR1-rhodanese-GroES complex. Elution profiles of analytical size exclusion chromatography of the rhodanese-SR1 complex (using singly acceptor-labeled rhodanese K135C) are shown at different times *t* after starting the refolding reaction by adding 1 μM GroES and 2 mM ATP. A TSK 5000 PWXL column (TOSOH Bioscience) with a flow rate of 0.8 ml/min and fluorescence detection was used (excitation at 585 nm, emission at 610 nm). The profile at *t* = 0 min is the size exclusion chromatography run before adding GroES and ATP. The peak at a retention time of 10 min corresponds to the chaperonin-rhodanese complex. Only very small amounts of free rhodanese (peak at 12.5 min) form over the course of the experiment. The increase in fluorescence of the peak corresponding to the chaperonin-rhodanese complex reflects the folding reaction inside the chaperonin cavity. The experiment was performed in folding buffer at room temperature.
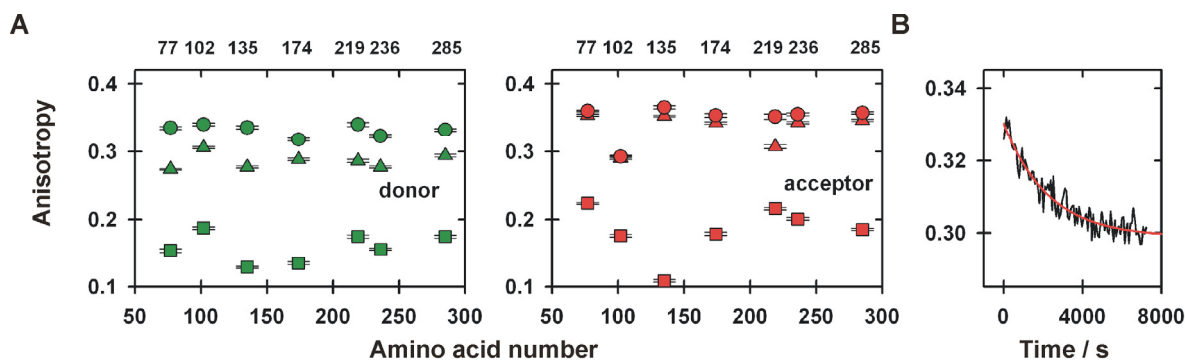
Fig. S2. Steady-state anisotropy measurements. (**A**) Single-cysteine variants of rhodanese were labeled either with the donor (green) or with the acceptor dye (red). Anisotropy values were recorded for free rhodanese (squares), binary rhodanese-SR1 complex (circles), and the encapsulated native rhodanese (triangles). (**B**) Kinetics of the change in donor anisotropy of the singly donor-labeled rhodanese variant K174C after addition of 1 μM GroES and 2 mM ATP at 22°C. The single exponential fit (solid line) yields a rate constant of $(4 \pm 1) \cdot 10^{-4}$ s^{-1}. The good agreement with the rate constants obtained from the single-molecule FRET experiments on doubly labeled protein [$(3.2 \pm 1.3) \cdot 10^{-4}$ s^{-1} for the N-variant and $(3.0 \pm 0.5) \cdot 10^{-4}$ s^{-1} for the L-variant at 22°C] supports the accuracy of the single molecule results and provides some indication that dye labeling does not affect the kinetics significantly (at least for AlexaFluor594, which is the larger chromophore). All measurements were performed in folding buffer.
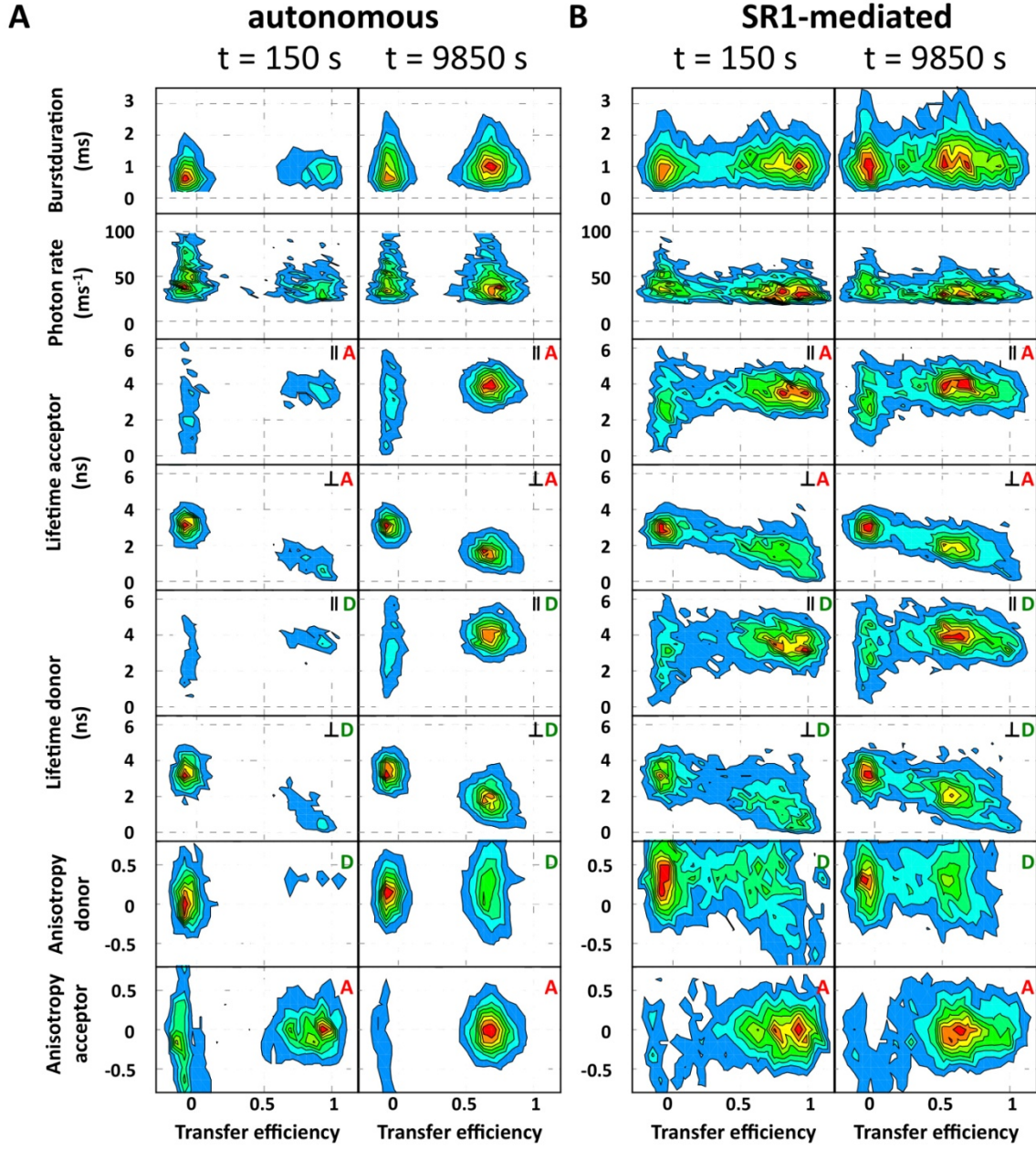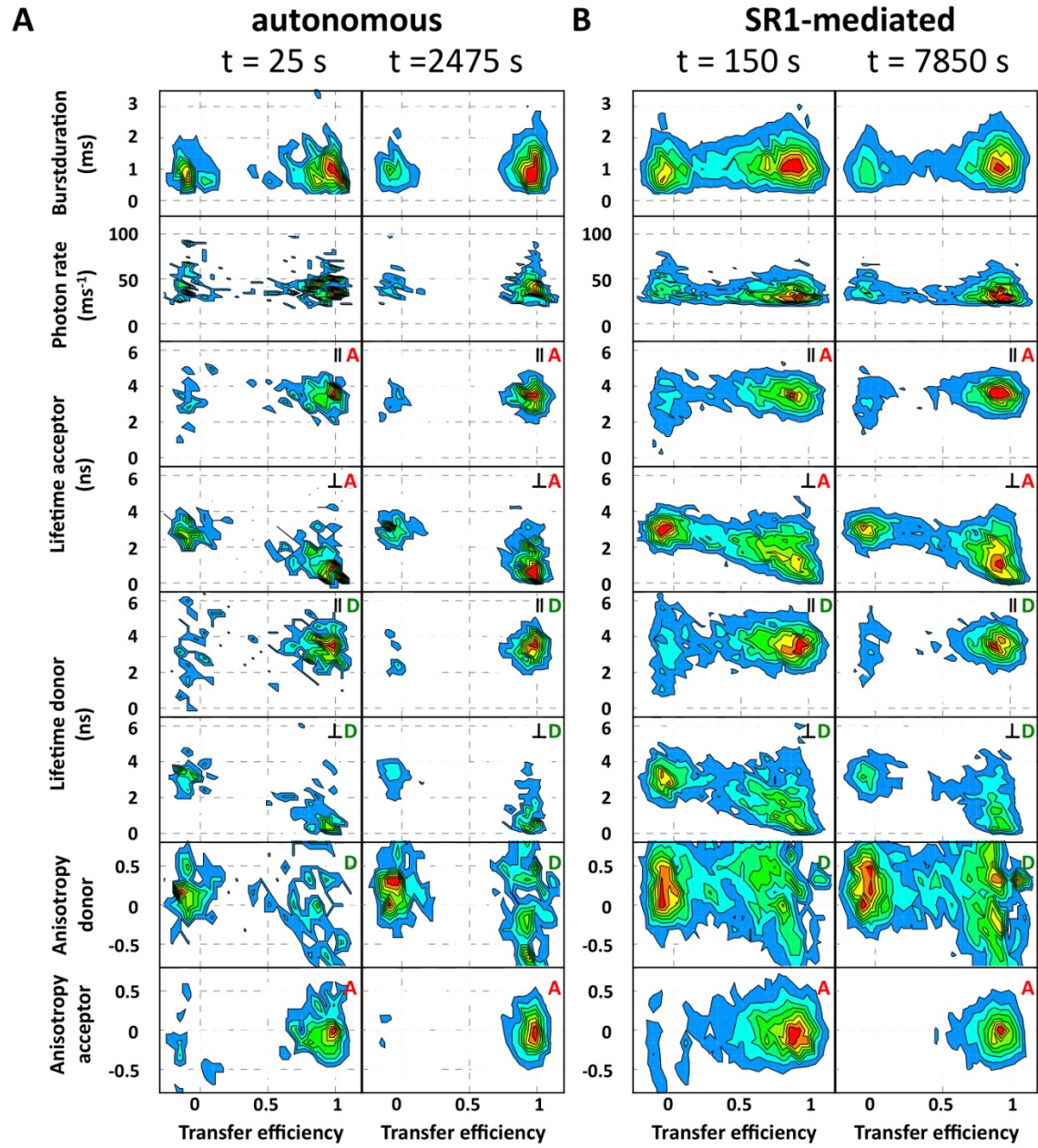
Fig. S3. 2D-Histograms for the autonomous **(A)** and SR1-mediated **(B)** folding reaction of the N-variant at the earliest (left) and latest (right) time point after starting the refolding reaction at 24°C.
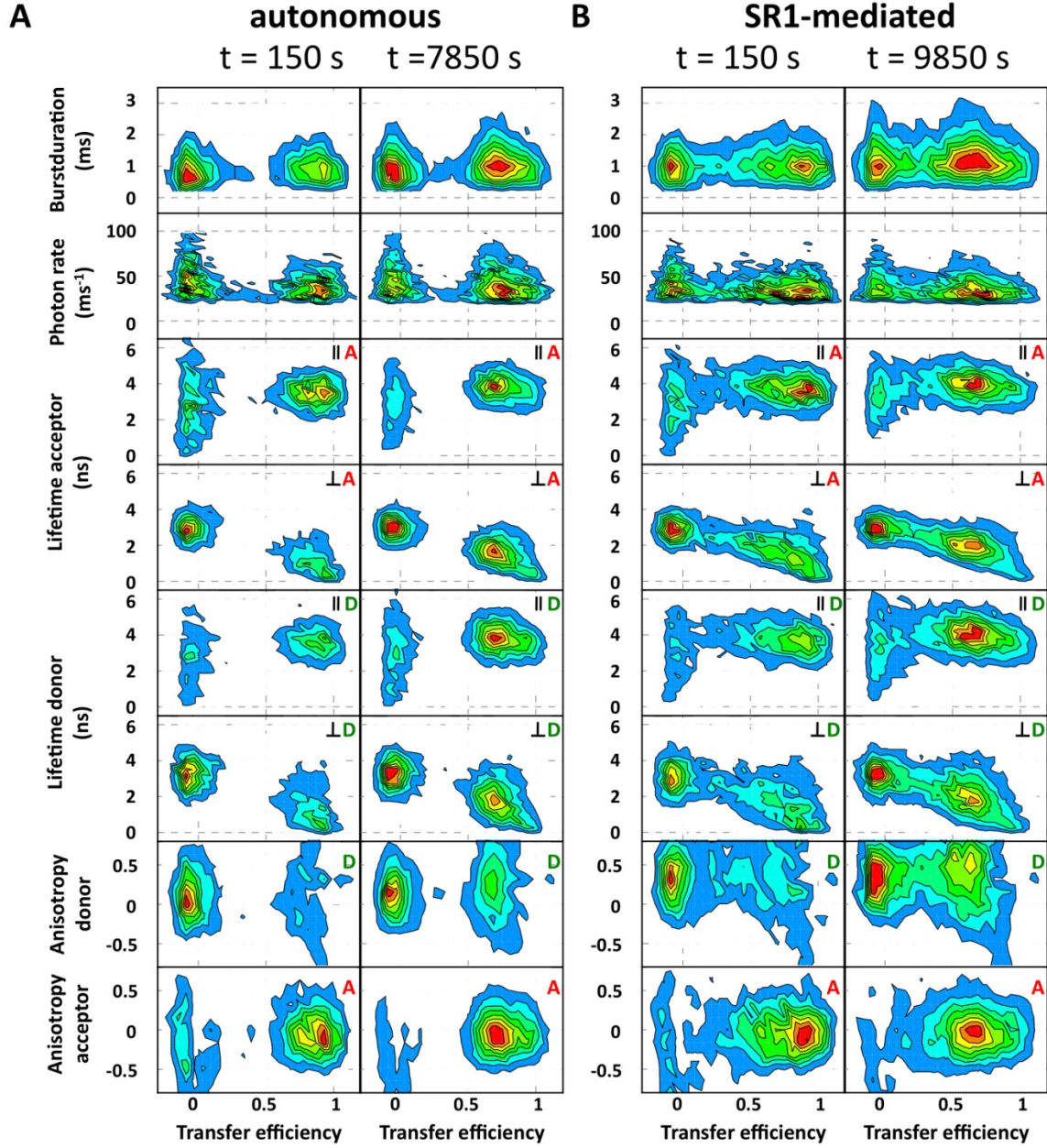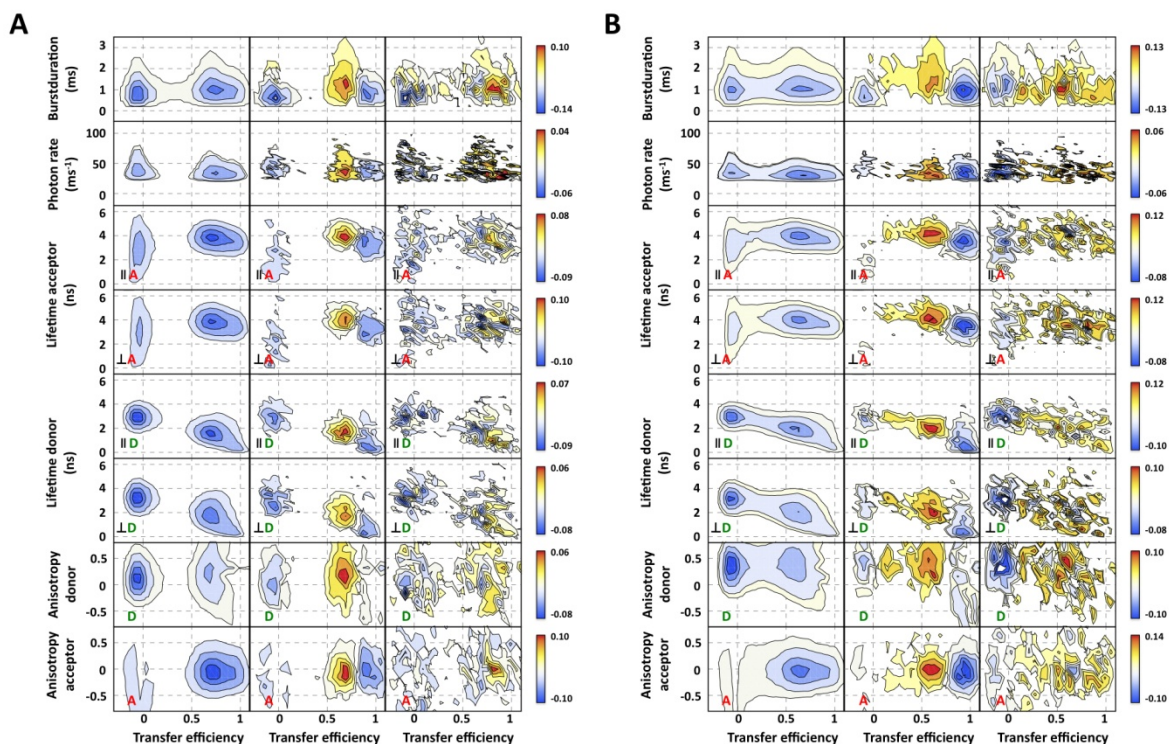
Fig. S4. 2D-Histograms for the autonomous **(A)** and SR1-mediated **(B)** folding reaction of the L-variant at the earliest (left) and latest (right) time point after starting the refolding reaction at 24°C.
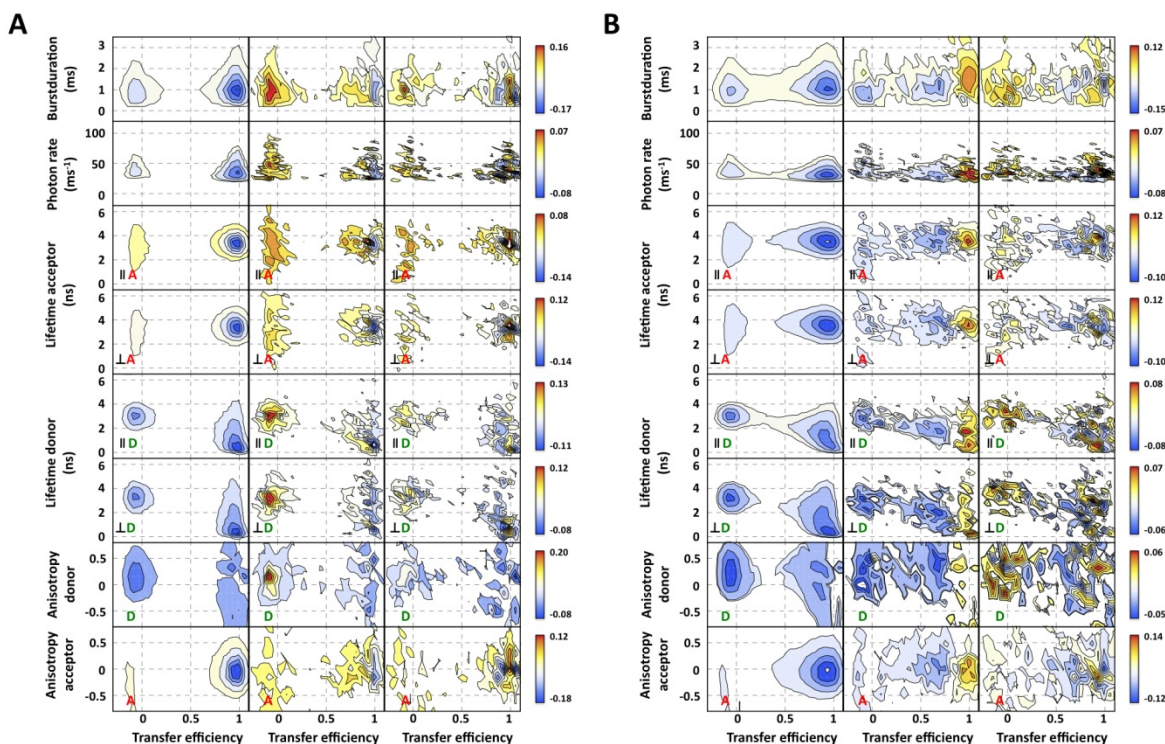
Fig. S5. 2D-Histograms for the autonomous **(A)** and SR1-mediated **(B)** folding reaction of the C-variant at the earliest (left) and latest (right) time point after starting the refolding reaction at 24°C.
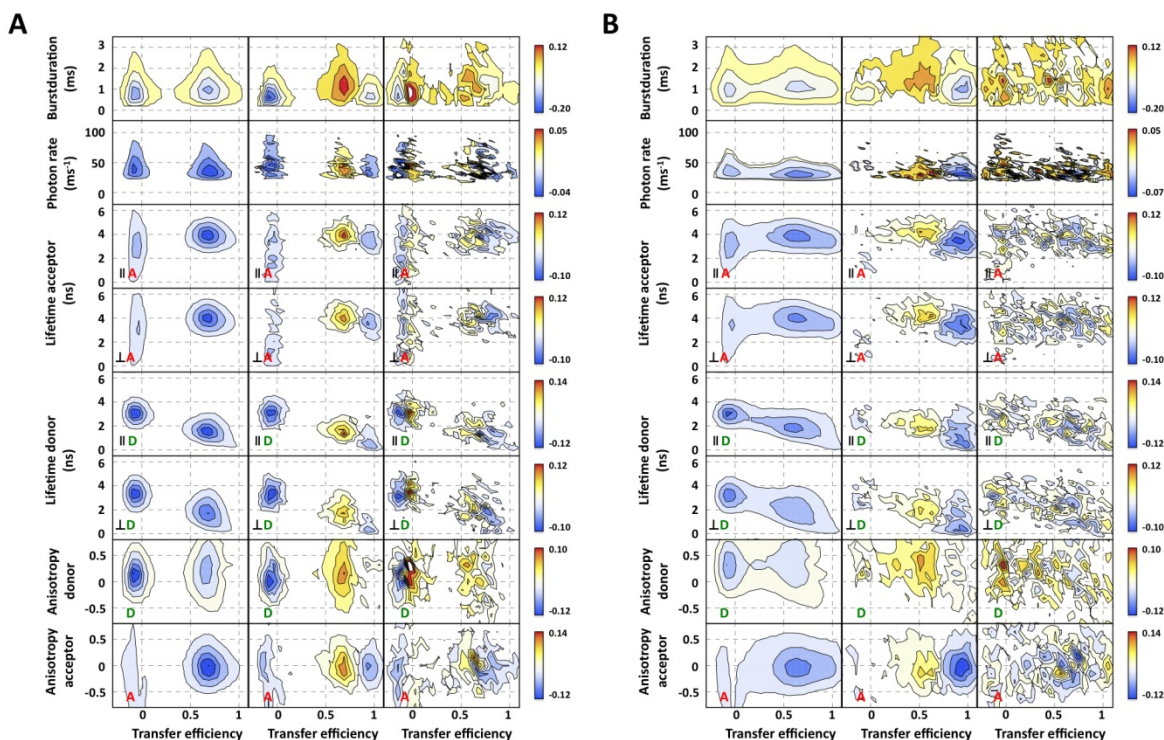
Fig. S6. Two-dimensional basis vectors of the multi-dimensional SVD for the spontaneous **(A)** and SR1-mediated **(B)** folding reaction of the N-variant at 24°C. The basis vectors indicate the positions of changes in the histograms of the corresponding observables (from top to bottom) and are ordered according to their singular values (from left to right). Basis vector 1 (left panel) describes an increase in the number of molecules during refolding. Basis vector 2 (middle panel) describes the conversion of the signature of non-native molecules (blue) to that of the native state (yellow and red). The larger noise level of basis vector 3 and the small corresponding singular values (see Fig. S9) for both the spontaneous (A) and the SR1-mediated folding reaction (B) indicate that the folding reaction is dominated by two distinguishable molecular species. The color code reflects the absolute SVD amplitude (see color scale).

Fig. S7. Two-dimensional basis vectors of the multi-dimensional SVD for the spontaneous **(A)** and SR1-mediated **(B)** folding reaction of the L-variant at 24°C. The basis vectors indicate the positions of changes in the histograms of the corresponding observables (from top to bottom) and are ordered according to their singular values (from left to right). Basis vector 1 (left panel) describes an increase in the number of molecules during refolding. Basis vector 2 (middle panel) describes the conversion of the signature of non-native molecules (blue) to that of the native state (yellow and red). The larger noise level of basis vector 3 and the small corresponding singular values (see Fig. S9) for both the spontaneous (A) and the SR1-mediated folding reaction (B) indicate that the folding reaction is dominated by two distinguishable molecular species. The color code reflects the absolute SVD amplitude (see color scale).

Fig. S8. Two-dimensional basis vectors of the multi-dimensional SVD for the spontaneous **(A)** and SR1-mediated **(B)** folding reaction of the C-variant at 24°C. The basis vectors indicate the position of a change in the histogram of the corresponding observable (from top to bottom) and are ordered according to their singular values (from left to right). Basis vector 1 (left panel) describes an increase in the number of molecules during refolding. Basis vector 2 (middle panel) describes the conversion of the signature of non-native molecules (blue) to that of the native state (yellow and red). The larger noise level of basis vector 3 and the small corresponding singular values (see Fig. S9) for both the spontaneous (A) and the SR1-mediated folding reaction (B) indicate that the folding reaction is dominated by two distinguishable molecular species. The color code reflects the absolute SVD amplitude (see color scale).
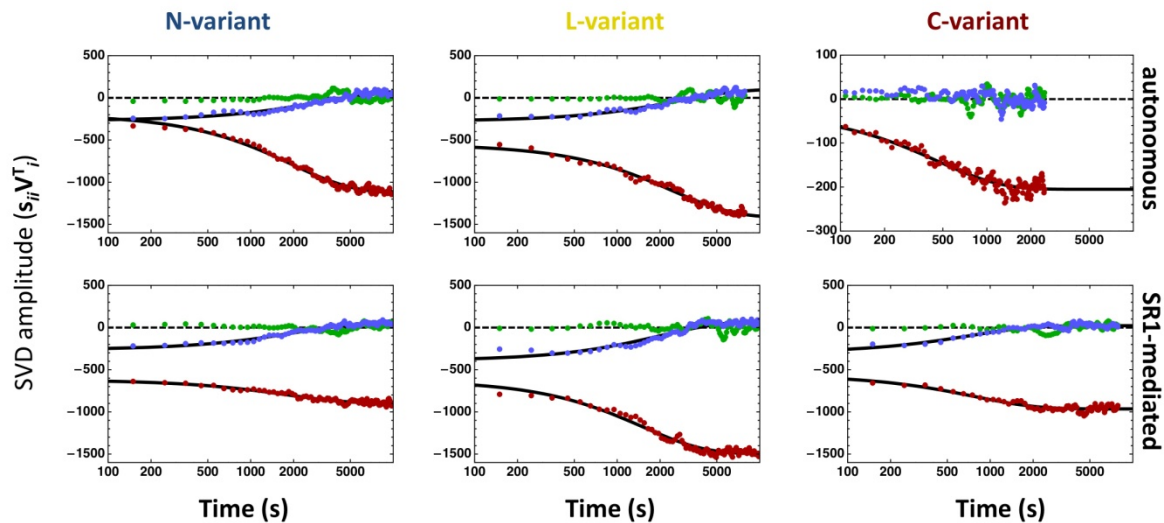
Fig. S9. First (red), second (blue), and third (green) amplitude vector weighted by their corresponding singular values (s_{ii}) of the multi-dimensional SVD for the spontaneous (upper panels) and SR1-mediated (lower panels) folding reaction of the N-, L-, and C-variants at 24°C. The first two amplitude vectors dominate the observed signal change.
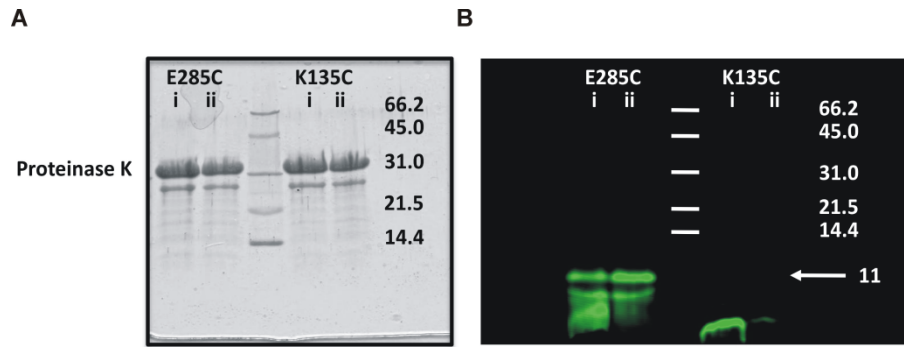
Fig. S10. Limited Proteolysis of singly-labeled rhodanese (K135C-D and E285C-D) indicates that the C-terminal domain folds prior to the N-terminal domain. **(A)** Coomassie stained SDS-Polyacrylamide gel (17%) of the proteolysis reaction mixture stopped at 100 s (i) and 300 s (ii) after addition of 2 mg/ml proteinase K. **(B)** Same gel, but scanned with an excitation wavelength of 488 nm.
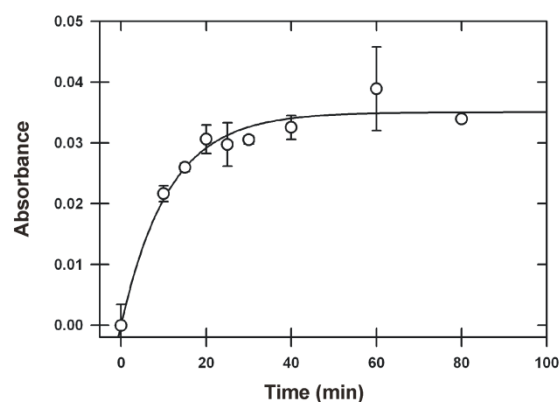
Fig. S11. Reactivation of doubly labeled rhodanese K135C/K174C by SR1. Enzymatic test as described in the supporting text. Error bars show standard errors of the means resulting from 3 independent measurements. A single-exponential fit yields a rate constant of 0.09 ± 0.04 min^{-1}, within the range of rate constants (from ~0.04 min^{-1} to ~0.16 min^{-1}) reported in the literature (14-17). The reactivation kinetics agree well with our single molecule results, especially considering the spread of previously reported values, the lack of temperature control for some of them, and the slow GroEL/ES dissociation step on ice required prior to the enzymatic test (13).
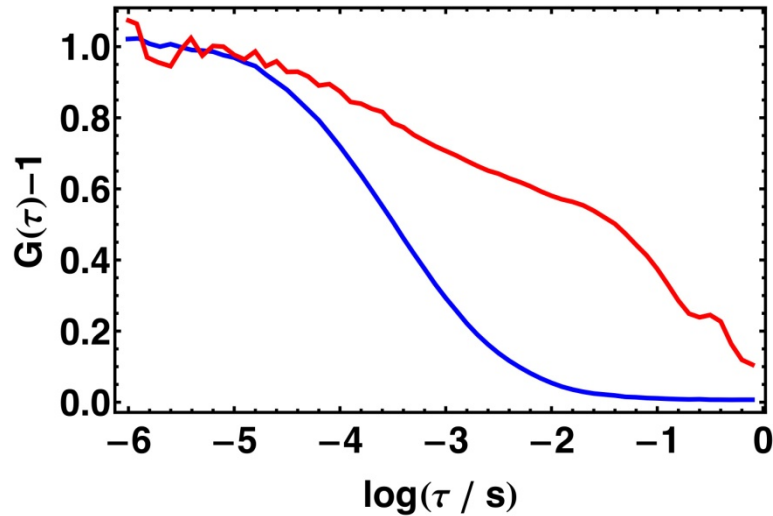
Fig. S12. Monitoring aggregation in single molecule experiments with fluorescence correlation spectroscopy. Under the experimental conditions and picomolar protein concentrations used in this work, no aggregation of rhodanese occurred, as illustrated by the normalized donor-acceptor fluorescence intensity cross-correlation function of the L-variant after initiation of refolding by manual mixing at 24°C (blue). The signatures of aggregated rhodanese previously observed in fluorescence lifetimes and burst size distributions (27) were also absent under these conditions. For comparison, a normalized cross-correlation function of rhodanese L-variant in the presence of an excess of unlabeled wildtype rhodanese is shown in red. The sample containing 4 nM labeled L-variant and 3 μM rhodanese wildtype was incubated for 2 minutes in 3 M urea. After dilution 1:50 into native conditions, the single molecule fluorescence time trace was recorded and the cross-correlation function calculated. The presence of aggregates leads to a heterogeneous distribution of translational diffusion times through the confocal volume and a correspondingly slower and in some cases even non-monotonic decay of the correlation function.